INTERNATIONAL JOURNAL FOR NUMERICAL METHODS IN FLUIDS
Int. J. Numer. Meth. Fluids 2005; **47**:451–469
Published online 14 December 2004 in Wiley InterScience (www.interscience.wiley.com). DOI: 10.1002/fld.825

Moving-interface computations with the edge-tracked interface locator technique (ETILT)

Marcela A. Cruchaga[1,*,†], Diego J. Celentano[1] and Tayfun E. Tezduyar[2,‡]

[1]*Departamento de Ingeniería Mecánica, Universidad de Santiago Chile, Av. Bdo. O'Higgins 3363, Santiago, Chile*
[2]*Team for Advanced Flow Simulation and Modeling (T*AFSM), Mechanical Engineering, Rice University-MS 321, Houston TX 77005, U.S.A.*

SUMMARY

We describe, for simulation of flows with moving interfaces, a computational method based on the edge-tracked interface locator technique (ETILT). The method described has been designed by bearing in mind the ease in managing a node-based interface representation and the interface sharpness and volume conservation features of the Moving Lagrangian Interface Technique. We evaluate the performance of the method with a number of test problems: filling of a step cavity, gravity-driven flow of an aluminium alloy in an obstructed channel, collapse of a liquid column, and the bore problem. Copyright © 2004 John Wiley & Sons, Ltd.

KEY WORDS: finite element computation; moving interfaces; edge-tracked interface locator technique

1. INTRODUCTION

Many engineering problems and manufacturing processes, such as channel flows or mould filling, require time-dependent analysis of flows with moving two-liquid interfaces or free surfaces. Development of computational tools needed to address the challenges present in this class of problems has been a major area of research interest. Specifically, dominant advective effects during the update of the moving interfaces, volume-conserving prediction of the interface location, and accurate computation in presence of large differences in material properties between the two fluids are some of the current issues.

*Correspondence to: Marcela A. Cruchaga, Departamento de Ingeniería Mecánica, Universidad de Santiago Chile, Av. Bdo. O'Higgins 3363, Santiago, Chile.
†E-mail: mcruchag@lauca.usach.cl
‡E-mail: tezduyar@rice.edu

Contract/grant sponsor: Chilean Council for Research and Technology; contract/grant numbers: 1020029, 7020029
Contract/grant sponsor: Department of Technological and Scientific Research, Universidade de Santiago de Chile

Received 25 March 2004
Revised 6 May 2004
Accepted 18 August 2004

Different numerical techniques have been proposed to analyse flow problems with moving interfaces and free surfaces. These can be categorized into two main groups: moving-mesh and fixed-mesh techniques. The arbitrary Lagrangian–Eulerian (ALE) technique [1, 2] and the deformable-spatial-domain/stabilized space–time (DSD/SST) method [3–5] are both moving-mesh formulations. In these methods the interface is tracked with the moving mesh, and the mesh is updated every time step to accommodate the tracking. Such techniques have good numerical accuracy, but the frequency of remeshing may become too high when complex and very unsteady interfaces need to be tracked. In an interface-capturing technique, on the other hand, typically a fixed mesh is used during the analysis by defining an interface function identifying the two fluids. The interface position is represented by the midpoint value of that interface function [6, 7]. The nodal values of this interface function (or pseudo-concentration function) are the additional unknowns in the problem, and a time-dependent advection equation governs the evolution of the interface function. Solution of the flow equations and the advection equation are based on stabilized formulations, and therefore the algorithm is rendered stable in the presence of dominant advective terms, without introducing excessive numerical dissipation. The stabilization also allows us to use equal-order interpolation functions for all unknowns involved. This class of methods has been successfully used, for example, in forming processes and mould filling analyses [8–11]. More recently additional research has focused on increasing the accuracy in representing the interface and better volume conservation [12–15]. Among them, the enhanced-discretization interface-capturing technique (EDICT) [12] was proposed as a way to enrich the interpolation near the interface. Other new methods and ideas developed to increase the scope and accuracy of interface-tracking and interface-capturing techniques were also described in References [12–15].

An alternative formulation based on using fixed finite element meshes consists of independently defining a surface mesh (1D in 2D cases and 2D in 3D cases) represented by additional marker points. The positions of these points are calculated at each time step by using a Lagrangian scheme, where different material properties are assigned at each side of the interface mesh [16–18]. Although reasonably satisfactory results were obtained with this method, some drawbacks in volume conservation were observed [18]. To improve the performance of this class of techniques, a global-mass-corrector algorithm has recently been developed. Moreover, since the material properties are not smooth within the elements crossed by the interface, an enhanced spatial integration technique has been developed to properly capture such material discontinuities. This improved method, which we call the moving Lagrangian interface technique (MLIT) [19, 20], has been applied to 2D analysis of two-fluid problems.

With the purpose of maintaining the ease in managing interfaces defined by a node-based approach and emulating the main features of the MLIT (i.e. interface sharpness and volume conservation) a new finite element approach, called the edge-tracked interface locator technique (ETILT), was introduced in Reference [12]. More recent versions of the ETILT were proposed in References [21–23]. In the present work we propose an algorithm based on the ETILT. The objective is to test the formulation by checking its numerical performance on problems with moving interfaces, to assess its main features, and to compare it with the existing techniques.

The proposed technique is briefly described in Section 2, where comments on its implementation and remarks on the observed numerical behaviour are included. In Section 3, we present four numerical examples: filling of a step cavity, gravity-driven flow of an aluminium alloy in an obstructed vertical channel, collapse of a liquid column, and the bore

problem. The results obtained are compared to those obtained with the MLIT and a standard interface-capturing technique, as well as those obtained in other numerical studies and also experimental investigations.

2. EDGE-TRACKED INTERFACE LOCATOR TECHNIQUE (ETILT)

In the ETILT, we define the interface position with an edge-tracked representation of the interface function, namely φ^{he}, such that the interfaces are represented by a collection of positions along the finite element edges crossed by the interfaces. Nodes of the finite element mesh belong to 'chunks' of Fluid 1 or Fluid 2. An edge either belongs to a chunk of Fluid 1 or Fluid 2 or it is crossed by the interface. Each element is either fully filled by a chunk of Fluid 1 or Fluid 2 or is shared by both. In this last case, the shares of Fluid 1 and 2 are determined by the position of the interface along the edges of that element. At each time step, given $\mathbf{u}_n^{\mathrm{h}}$ and φ_n^{he} for the time level n, we determine $\mathbf{u}_{n+1}^{\mathrm{h}}$, $\mathrm{p}_{n+1}^{\mathrm{h}}$ and $\varphi_{n+1}^{\mathrm{he}}$, where $\mathbf{u}$ and p are the velocity and pressure respectively. The Navier–Stokes equations are solved using a generalized streamline operator technique as described in References [17, 18]. The density and viscosity, ρ and μ, used in the Navier–Stokes equations are expressed based on the edge-tracked representation of the interface function:

$$\rho^{\mathrm{h}} = \varphi^{\mathrm{he}}\rho_1 + (1 - \varphi^{\mathrm{he}})\rho_2 \tag{1}$$

$$\mu^{\mathrm{h}} = \varphi^{\mathrm{he}}\mu_1 + (1 - \varphi^{\mathrm{he}})\mu_2 \tag{2}$$

In marching from time level n to n+1, given φ^{he}, we first calculate a nodal representation φ^{h}, for example by using a least-squares projection:

$$\int_\Omega \psi^{\mathrm{h}}(\varphi_n^{\mathrm{h}} - \varphi_n^{\mathrm{he}})\,\mathrm{d}\Omega = 0 \tag{3}$$

where ψ^{h} is the test function. A projection of the kind given by Equation (3) is carried out so that we can update the interface by using the advection equation that governs φ:

$$\partial\varphi/\partial\mathrm{t} + \mathbf{u}\cdot\partial\varphi/\partial\mathbf{x} = 0 \tag{4}$$

To compute $\varphi_{n+1}^{\mathrm{h}}$, we use the discretized form of Equation (4). From $\varphi_{n+1}^{\mathrm{h}}$ we obtain $\varphi_{n+1}^{\mathrm{he}}$ by a combination of a least-squares projection:

$$\int_\Omega (\psi_{n+1}^{\mathrm{he}})_{\mathrm{P}}((\varphi_{n+1}^{\mathrm{he}})_{\mathrm{P}} - \varphi_{n+1}^{\mathrm{h}})\,\mathrm{d}\Omega = 0 \tag{5}$$

and corrections to enforce volume conservation for chunks of Fluid 1 and 2. This volume conservation condition among the fluid chunks can symbolically be written as

$$\mathrm{VOL}(\varphi_{n+1}^{\mathrm{he}}) = \mathrm{VOL}(\varphi_n^{\mathrm{he}}) \tag{6}$$

The subscript P in Equation (5) is used for representing the intermediate values following the projection, but prior to the corrections for the volume conservation. In addition, ψ^{he} is the test function associated with φ^{he}. In the remainder of this section we provide more details of the implementation.

Based on Equation (5), we write $(\varphi^{\mathrm{he}}_{n+1})_{\mathrm{P}} = H(\varphi^{\mathrm{h}}_{n+1} - 0.5)$, where H is the Heaviside function. In this case, $(\psi^{\mathrm{he}}_{n+1})_{\mathrm{P}} = \delta(\varphi^{\mathrm{h}}_{n+1} - 0.5)$, where δ is the Dirac function. We approximate the volume conservation condition given by Equation (6) with its global version, as given by the following equation:

$$\int_{\Omega} (\varphi^{\mathrm{he}}_{n+1} - \varphi^{\mathrm{he}}_{n})\,\mathrm{d}\Omega = Q \tag{7}$$

where Q is the mass inflow/outflow in the time interval $[n, n+1]$. An iterative procedure is employed to satisfy Equation (7). The mass balance ratio is defined as

$$R_m = \left(\int_{\Omega} (\varphi^{\mathrm{he}}_{n+1} - \varphi^{\mathrm{he}}_{n})\,\mathrm{d}\Omega\right) \Big/ Q \tag{8}$$

for $Q \neq 0$, and as

$$R_m = \left(\int_{\Omega} \varphi^{\mathrm{he}}_{n+1}\,\mathrm{d}\Omega\right) \Big/ \left(\int_{\Omega} \varphi^{\mathrm{he}}_{n}\,\mathrm{d}\Omega\right) \tag{9}$$

for $Q = 0$. The residual R_m needs to be equal to 1.0 for volume conservation. To achieve this $\varphi^{\mathrm{h}}_{n+1}$ is corrected iteratively as follows:

$$\varphi^{\mathrm{h}}_{n+1,i+1} = \varphi^{\mathrm{h}}_{n} + (\varphi^{\mathrm{h}}_{n+1,i} - \varphi^{\mathrm{h}}_{n})/(R_m)^k \tag{10}$$

where $k = \mathrm{sign}(\varphi^{\mathrm{h}}_{n+1,i} - \varphi^{\mathrm{h}}_{n})$ and i is the iteration counter. An alternative correction algorithm can be written as $\varphi^{\mathrm{h}}_{n+1,i+1} = \varphi^{\mathrm{h}}_{n+1,i} + |\varphi^{\mathrm{h}}_{n+1,i} - \varphi^{\mathrm{h}}_{n}|(1.0 - R_m)$. The iterations continue until the volume conservation condition is reached, i.e. $|R_m - 1.0| < \varepsilon_R$, where ε_R is an acceptable tolerance. When the convergence is reached, $\varphi^{\mathrm{h}}_{n+1}$ generates a volume-conserving value for $\varphi^{\mathrm{he}}_{n+1}$. This value serves as the starting point for the computations in marching from $n+1$ to $n+2$.

Remark 1

The projection specifically given by Equation (3) is a consistent way of reconstructing φ^{h} from φ^{he}. In addition to this consistency, we need φ^{h} to have a value of 0.5 at the interface. Equation (3), by itself, does not ensure that. Projection techniques that do satisfy this requirement were recently proposed in References [21–23]. In this paper, as a shortcut, we skip the projection in the elements crossed by the interface. This means that the converged value of φ^{h} coming from the iterations given by Equation (10) is preserved in regions near the interface. With this approach, the φ^{h} obtained from the projection maintains a value of 0.5 at the interface and is still sharp to a certain degree. Nevertheless, the occasional use of Equation (3) also near the interface is useful to smooth φ^{h} at times it exhibits excessive oscillations near to the interface. The error introduced by such occasional projections is practically negligible in a transient analysis.

Remark 2

The volume conservation corrections can be made in two different ways: adjusting the locations of the interface along the edges [12] or adjusting the value of the node-based representation of the interface. In this work we selected the second alternative.

Remark 3
A sub-element integration technique is used for accurately carrying out the spatial integrations over the elements crossed by the interface. The sub-elements can be generated by a regular subdivision [19, 20]. They can also be generated by a subdivision along the interface, which is more straightforward in the ETILT than it is in the MLIT. According to our experience in computation of the type of problems we consider here, the two subdivision approaches yield very comparable results. Defining the fluid properties as given by Equations (1) and (2), together with the sub-element integration approach, is one of the unique features of the ETILT. Furthermore, techniques based on smoother interface functions (see References [6–11]), including the level set techniques (which are based on a distance function), require periodically reconstructing the interface function (or the distance function). This is automatically taken care of in the ETILT with Equation (3). On the other hand, with respect to the solution of the advection equation, the ETILT involves mesh and time-step size limitations similar to those involved in techniques based on smoother interface functions.

Remark 4
As we march from time level n to $n+1$, we solve the Navier–Stokes equations based on the interface position at time level n, without updating the interface during the non-linear iterations. Following that, and using the velocity field just computed for time level $n+1$, we calculate the interface position at $n+1$. We then move on to the next time step. In the ETILT, with its original way of handling the coupling between the Navier–Stokes and interface update equations (see References [12, 21–23]), the interface update is embedded in the non-linear iterations of the Navier–Stokes equations. According to our experience with computation of the type of problems we report here, the original coupling approach and its approximate version we use here give similar results. We use backward difference time-integration for both the Navier–Stokes and advection equations. For the problems we consider here, we observe no significant variations in the results if we instead use central differencing for either of the two equations or for both.

Remark 5
How the wall boundary conditions are handled influences the interface motion. We see a number of approaches in the literature (see for example References [6–11]), such as using high mesh refinement near the wall or using a frictional wall law. Assuming that the inertial effects are dominant over the viscous ones and using, for simplicity, free-slip boundary conditions is also quite common in the literature (see References [6–11]). We provide some brief comments in Section 3.3 based on a comparative evaluation of both the free- and no-slip conditions.

3. NUMERICAL EXAMPLES

3.1. Filling of a step cavity

This problem was proposed in Reference [8] as a simple test for mould filling, and it was computed in Reference [20] to evaluate the performance of the MLIT in open systems. The problem layout is shown in Figure 1. Initially the front of the filling material (Fluid 1) is located at $x = 0.02$ m inside the lower step mould, while the rest of the cavity is occupied by air (Fluid 2). Both fluids are initially at rest. A uniform velocity profile of 0.1 m/s is imposed

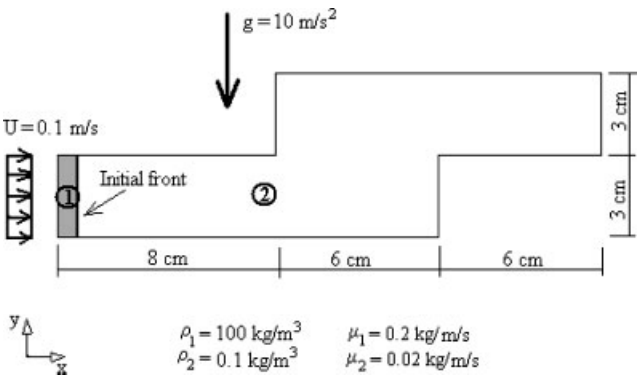

Figure 1. Filling of a step cavity. Problem layout.

at the inflow boundary, and traction-free conditions are imposed at the outflow boundary. Free slip conditions are assumed at the walls. The fluid material properties, obtained from Reference [8], are also given in Figure 1. The domain is discretized with a uniform finite element mesh composed of 700 isoparametric four-noded (bilinear) elements. The time step size used in the computations is 0.01 s.

The results obtained with the ETILT are compared with those obtained with the MLIT and the standard interface-capturing technique. The MLIT has an interface mesh defined with 60 points, and the standard technique is the one described [6], with no redefinition of the interface during the transient analysis.

Figure 2 shows the front positions at various instants during the simulation. In the early stages, the low inflow velocity allows the front to spread under the influence of the gravity. In those stages, the horizontal motion of the front near the upper wall is diminished because the effect of the inflow velocity is reduced by the effect of the gravity. After the front reaches the vertical wall of the lower step, the height of the filling material becomes nearly uniform until $t = 1.0$ s. Then, the effect of the sudden change in the flow direction becomes apparent, and the upper step starts filling. The material moves along the vertical wall of the upper step. Soon after that a channel flow develops as the material exits through the outflow boundary. At $t = 2.5$ s a nearly steady state is reached. Overall, a reasonably good agreement between the three techniques can be observed. In particular, the results obtained with the ETILT agree very well with those obtained with the MLIT. We note that the oscillations seen in some regions in solutions obtained with the standard interface-capturing technique are not present in the solutions obtained with the ETILT.

Figure 3 shows the contours of φ^{h} at various instants. The interface-sharpening effect of the projection given by Equation (3) can clearly be noted for the ETILT results.

3.2. *Gravity-driven flow of an aluminium alloy in an obstructed vertical channel*

The problem set up is shown in Figure 4. Initially the alloy front is at $h_0 = 0.09$ m (at the top of the channel $h = 0.1$ m). The rest of the channel is occupied by air. Both fluids are initially at rest. Traction-free conditions are imposed at both the inflow and outflow boundaries. Slip

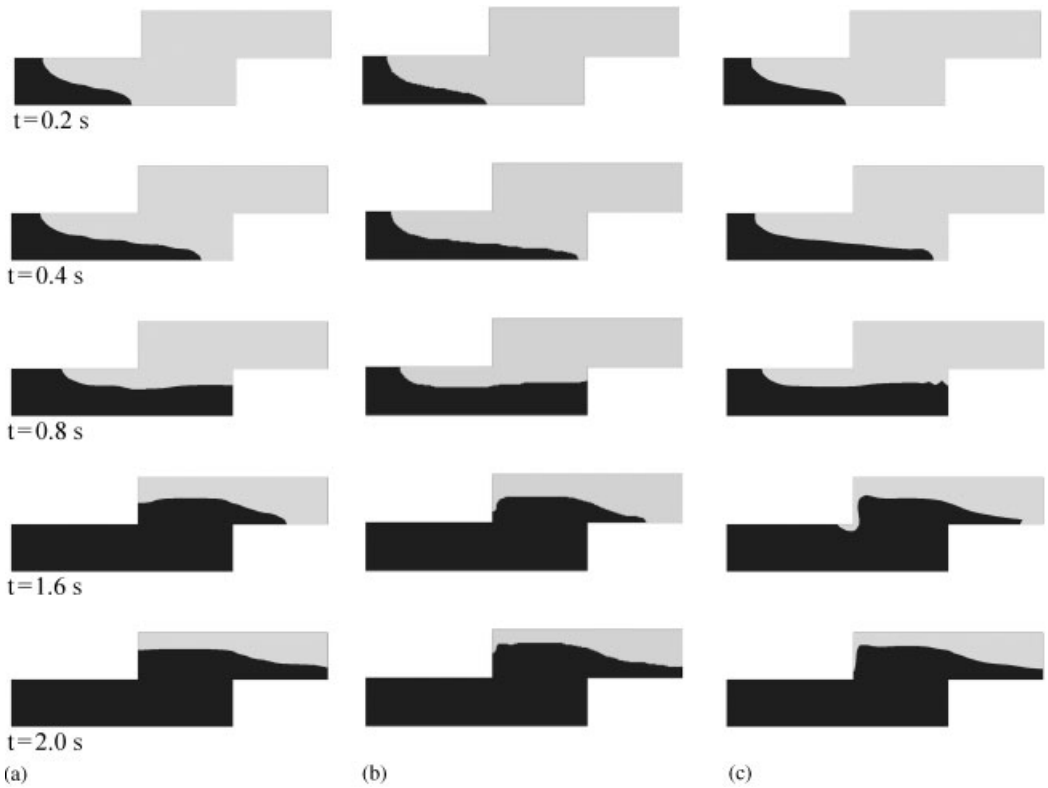

Figure 2. Filling of a step cavity. Interface positions at various instants, obtained with (a) the ETILT, (b) MLIT, and (c) the standard technique.

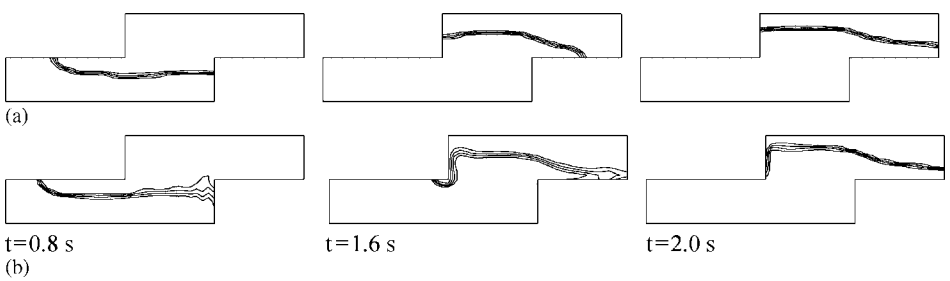

Figure 3. Filling of a step cavity. Contours of φ^h at various instants, obtained with (a) the ETILT, and (b) the standard technique.

boundary conditions are assumed at the walls. The fluid material properties are also shown in Figure 4. For the viscosity of the air, a value 100 times the actual one is used to prevent numerical oscillations caused by the turbulent air flow. Actual physical values are used for all other fluid properties. The finite element mesh used has 1900 isoparametric four-noded

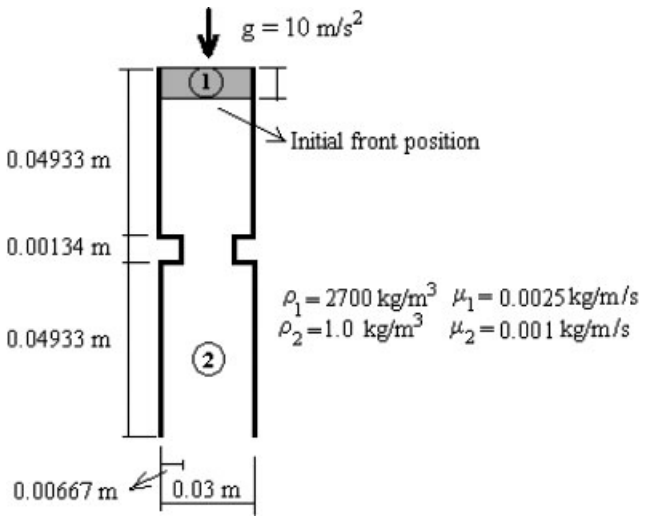

Figure 4. Gravity-driven flow of an aluminium alloy in an obstructed vertical channel. Problem layout.

elements. The minimum time step size is 0.001 s. The results are compared with those obtained with the MLIT, using a moving interface mesh composed of 20 points.

Figure 5 shows the front positions at various instants. Before the alloy reaches the obstruction, the front motion is primarily governed by a friction-free particle motion, where the position and the velocity can be expressed as $h_0 - 0.5gt^2$ and $-gt$, respectively. The air velocity through the obstruction increases. As the air is compressed in the upper side of the obstruction wall ($t = 0.080$ s), a sudden increase in the horizontal component of the air velocity occurs in this zone. The front accelerates and an alloy jet starts to develop. Then, the front continues to move downward, surrounded by air with high induced vortices. The alloy reaches the outflow boundary at $t = 0.117$ and 0.113 s for the MLIT and ETILT simulations, respectively. Overall, there is a reasonably good agreement between the ETILT and MLIT solutions.

Figure 6 shows the time evolution of the front position and velocity along the vertical central line. It can be seen that initially the front moves like a friction-free particle. Parabolic and linear profiles are obtained respectively for the position and velocity, until around $t = 0.09$ s. This is consistent with the assumption of slip conditions at the walls and negligible pressure gradient in the alloy. This trend is captured slightly better by the MLIT solution. When the filling material crosses the obstruction, we see a sudden increase in the velocity, inversely proportional to the ratio of the gap and channel widths. For both the MLIT and ETILT simulations, the front accelerates at such a level that the bottom of the channel is reached in less time than what we would have for a friction-free particle model (0.134 s).

3.3. *Collapse of a liquid column*

Due to the availability of experimental data [25, 28] for this problem, several researchers [24, 26, 27] used it as a test case to check the performance of the methods they were using. The problem layout is shown in Figure 7. In this paper we consider two configurations: an open receptacle with a liquid column 'slenderness' ratio of 1.0, and a closed receptacle

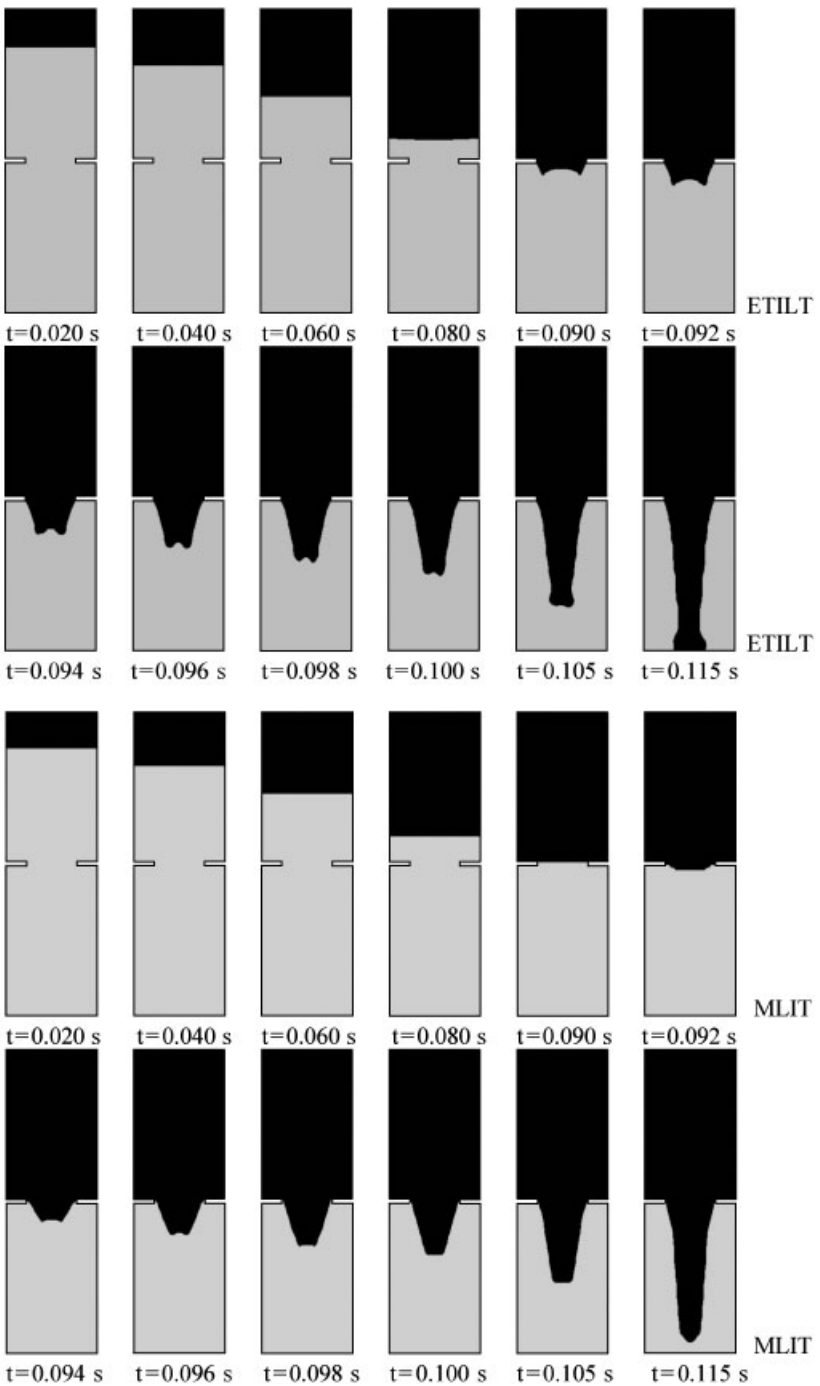

Figure 5. Gravity-driven flow of an aluminium alloy in an obstructed vertical channel. Interface positions at various instants, obtained with the ETILT and MLIT.

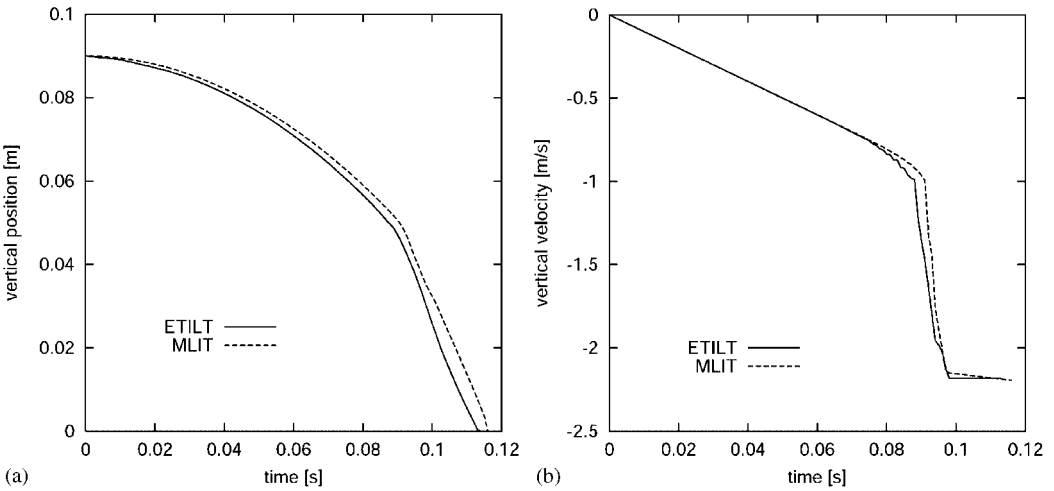

Figure 6. Gravity-driven flow of an aluminium alloy in an obstructed vertical channel. Time evolution of the front position (a) and velocity (b) along the vertical central line.

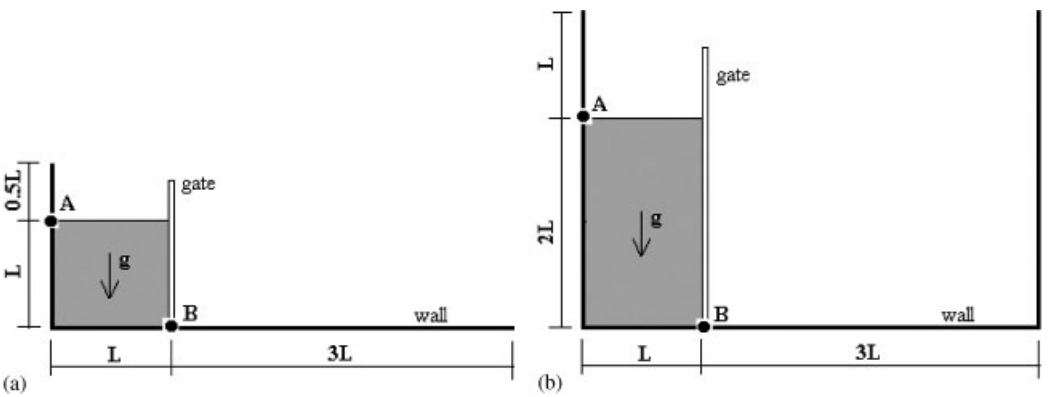

Figure 7. Collapse of a liquid column. Problem layout for open (a) and closed (b) receptacle.

with 2.0. The column width is $L = 0.05715$ m. The liquid column is initially at rest and confined between the left wall and the 'gate' that is assumed to be suddenly removed at time $t = 0$ s. Slip conditions are assumed at the solid surfaces and the pressure is set to zero at the top of the rectangular computational domain. The fluid properties used in our computations are those reported in Reference [24]: $\rho_1 = 1000\,\mathrm{kg/m^3}$ and $\mu_1 = 0.5\,\mathrm{kg/m/s}$ for the liquid, and $\rho_2 = 1\,\mathrm{kg/m^3}$ and $\mu_2 = 0.001\,\mathrm{kg/m/s}$ for the gas. The time step size used in the calculations is 0.001 s.

3.3.1. Open receptacle. The time evolution of the front position at the bottom wall (point B in Figure 7) is shown in Figure 8. The plots are in dimensionless time, $t(g/L)^{1/2}$, and dimensionless position, x/L. For both the ETILT and MLIT, the finite element mesh ('fine

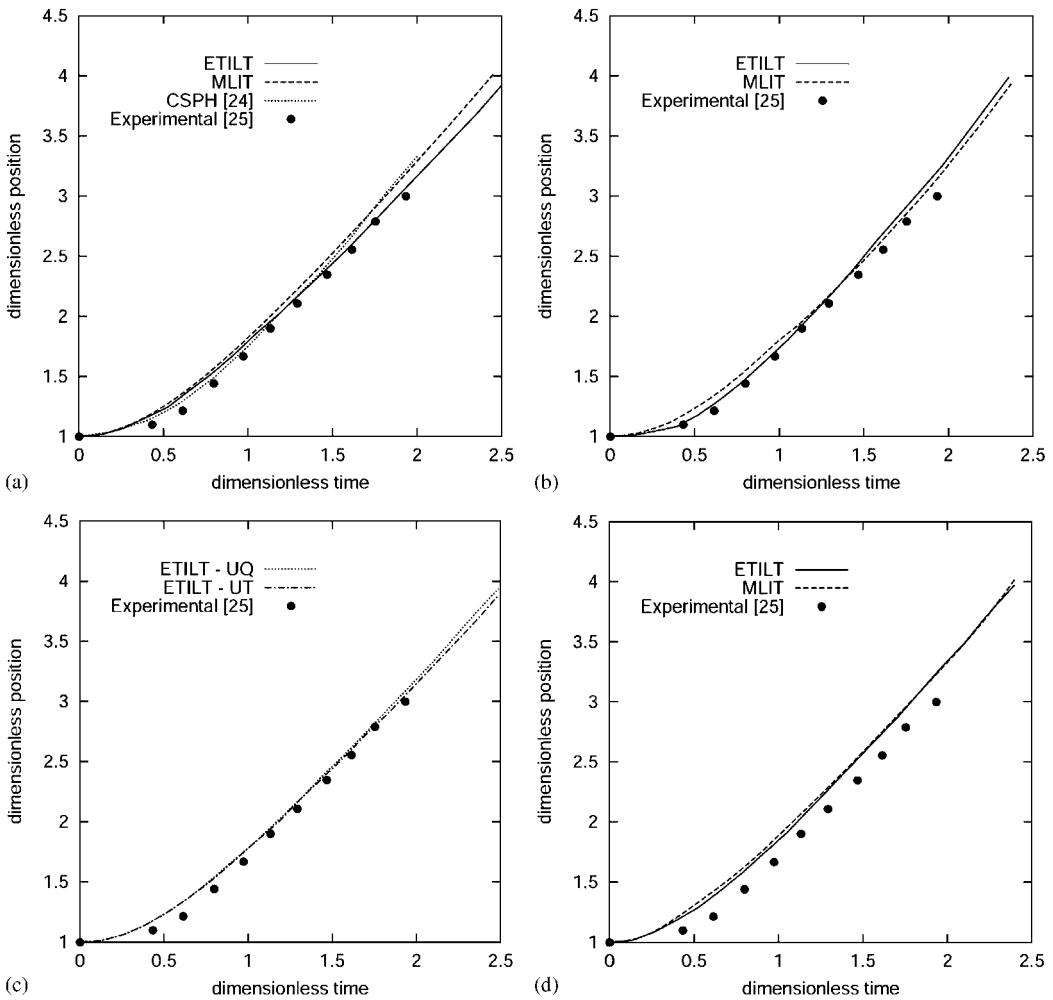

Figure 8. Collapse of a liquid column in an open receptacle. Time evolution of the front position at the bottom wall (point B): (a) fine mesh and $\mu_1 = 0.5$ kg/m/s, (b) coarse mesh and $\mu_1 = 0.5$ kg/m/s, (c) fine unstructured meshes (UQ: quadrilaterals and UT: triangles) and $\mu_1 = 0.5$ kg/m/s, and (d) fine mesh and $\mu_1 = 0.001$ kg/m/s.

mesh') is uniform and has 120×45 isoparametric four-noded elements. The MLIT has a moving interface mesh defined with 40 points. The results are shown in Figure 8(a) together with those obtained with a smooth particle hydrodynamic formulation (CSPH) [24] and those obtained experimentally [25]. Very similar results are obtained with a 'coarse mesh' composed of 40×15 elements (see Figure 8(b)). Figure 8(c) shows the numerical results obtained by using unstructured meshes composed of quadrilateral and triangular elements, which are very comparable. These results are also very comparable to those shown in Figures 8(a) and 8(b). Computations were carried out also with $\mu_1 = 0.001$ kg/m/s. In this case convergence was achieved only with the fine mesh. The ETILT and MLIT results, which are very close, are

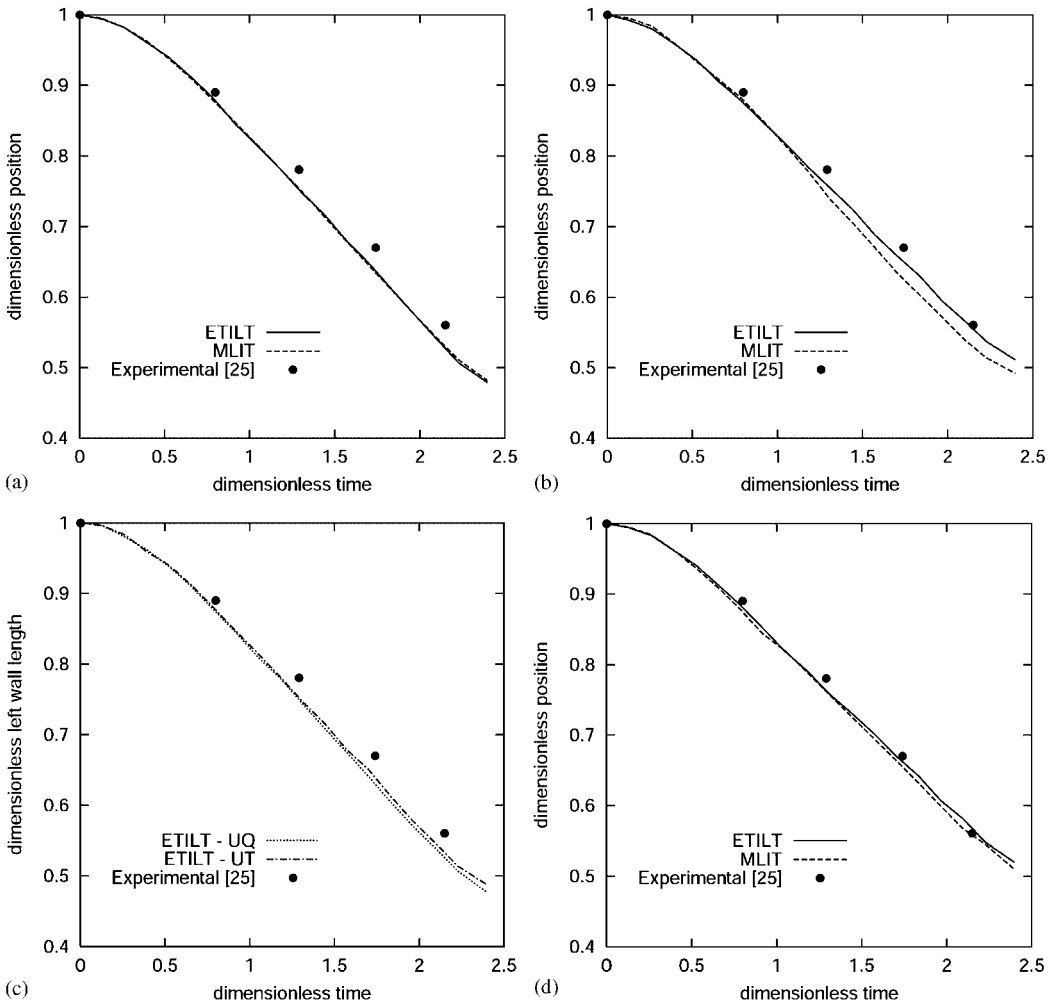

Figure 9. Collapse of a liquid column in an open receptacle. Time evolution of the front position at the left wall (point A): (a) fine mesh and $\mu_1 = 0.5\,\text{kg/m/s}$, (b) coarse mesh and $\mu_1 = 0.5\,\text{kg/m/s}$, (c) fine unstructured meshes (UQ: quadrilaterals and UT: triangles) and $\mu_1 = 0.5\,\text{kg/m/s}$, and (d) fine mesh and $\mu_1 = 0.001\,\text{kg/m/s}$.

shown in Figure 8(d). We note that the discrepancy in the positions predicted numerically and measured experimentally is almost constant. This discrepancy corresponds to a time lag of approximately 0.008 s (0.1 in dimensionless time) between the experimental and numerical results. If we shift the numerical results to the right (or the experimental results to the left) by approximately 0.1 dimensionless time unit, we obtain a picture very similar to what we see in Figure 8(a) for the ETILT. Because of this, we think that the slight discrepancy might be due to the start up conditions. The time evolution of the front position at the left wall (point A) is shown in Figure 9. The results obtained with the ETILT and MLIT are in good agreement

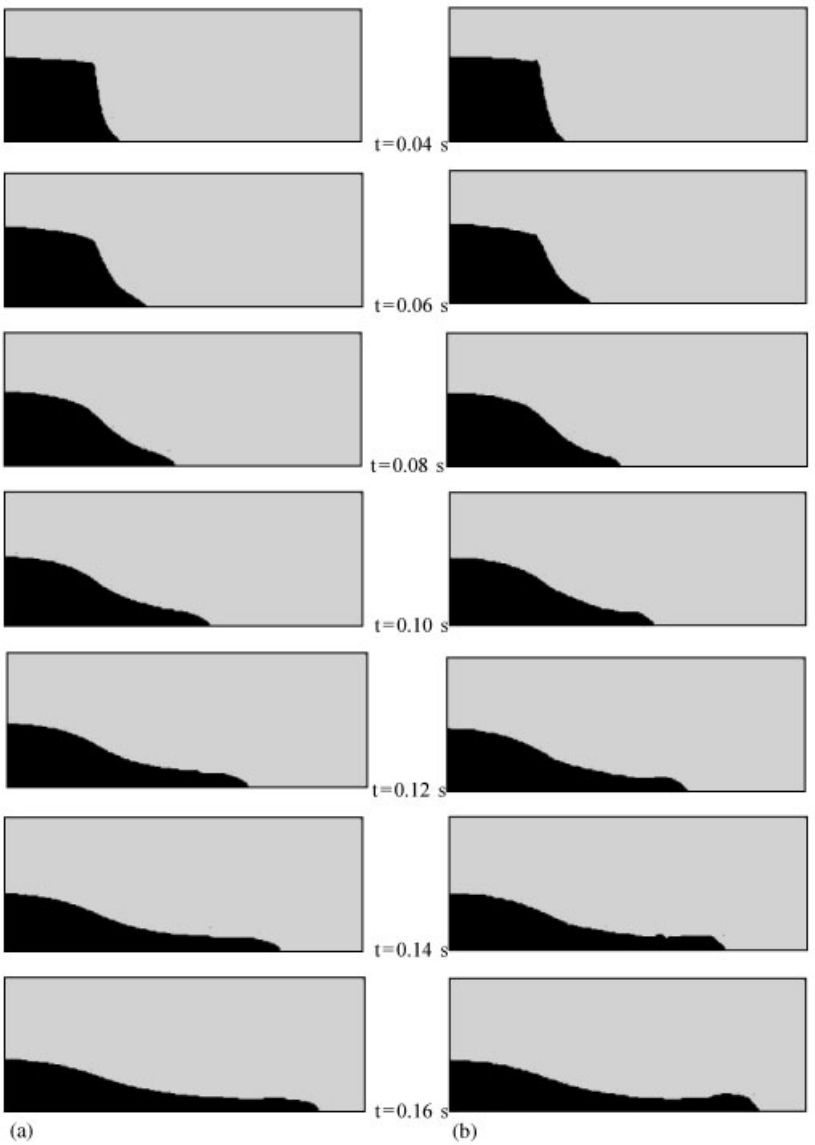

Figure 10. Collapse of a liquid column in an open receptacle. Interface positions at various instants, obtained with (a) the ETILT, and (b) MLIT.

with the experimental results [25]. The interface positions at various instants computed with the ETILT and MLIT are shown in Figure 10. They show qualitatively good agreement with the numerical [24] and experimental [25, 28] results. We repeated the computations for $\mu_1 = 0.001$ kg/m/s with a time step 10 times larger (0.01 s). With this large time step size, while the MLIT computations converge, the ETILT computations do not. Better understanding of this particular behaviour of the ETILT is one of our future topics of investigation.

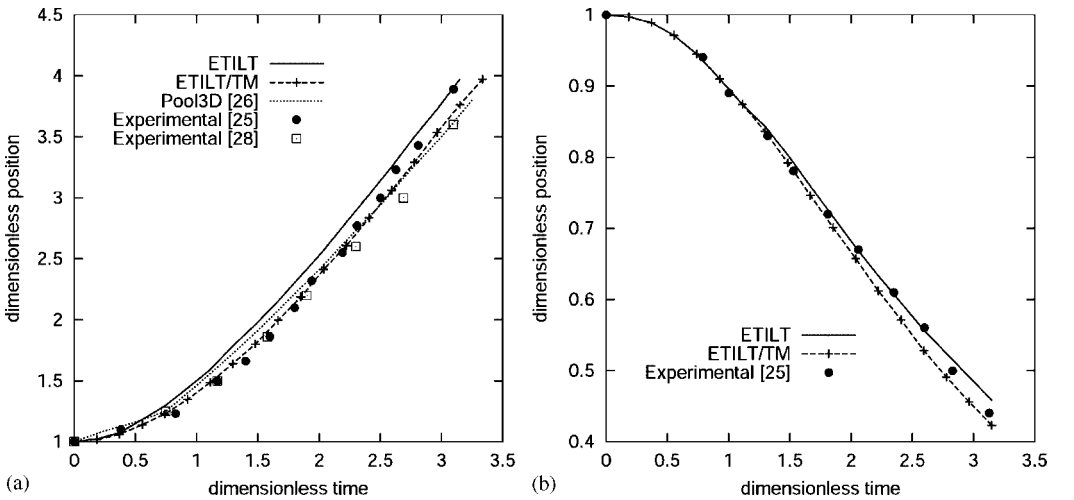

Figure 11. Collapse of a liquid column in a closed receptacle. Time evolution of the front position (a) at the bottom wall (point B) and (b) at the left wall (point A).

For a brief, comparative evaluation of the free-slip and no-slip conditions on the wall, in a separate test computation we changed the free-slip conditions to the no-slip conditions. With that we used higher mesh refinement near the wall. We observed that the corresponding results obtained with the ETILT (not shown here) are very comparable to those shown in Figures 8–10.

3.3.2. Closed receptacle. The time evolution of the front position at the bottom wall (point B), obtained with the ETILT is shown in Figure 11(a). The results are compared with those obtained with another numerical method, POOL3D [26], and from experiments [25, 28]. In this case the dimensionless time is $t(2g/L)^{1/2}$. The finite element mesh is uniform and has 120×90 four-noded elements. The computations are carried out with $\mu_1 = 0.001$ kg/m/s. We compute with the ETILT and also with the ETILT with a turbulence model ('ETILT/TM'). In the ETILT/TM, for both fluids, we use as viscosity $\min(\mu + \rho(l_{\text{mix}})^2\gamma, \mu_{\max})$, where l_{mix} is the mixing length that is taken here as the vortex length, and γ is the effective strain rate, $\sqrt{(2/3)\varepsilon : \varepsilon}$, where ε is the strain-rate tensor. For both fluids, we set $l_{\text{mix}} = 0.010$ m, and set $\mu_{\max}$ to 3.0 kg/m/s for Fluid 1 and 1.0 kg/m/s for Fluid 2.

Figure 11(b) shows the time evolution of the front position at the left wall (point A). For both point B and point A, the ETILT results are in good agreement with the experimental results [25].

Although the ETILT with no turbulence model predicts slightly more advanced front positions at the bottom wall, overall the flow patterns look reasonable until the liquid impinges on the right wall. After that point in time, the front unrealistically climbs up the wall as seen in Figure 12. The results obtained with the ETILT/TM for the same time period are also shown in Figures 12, and for time periods beyond that in Figure 13. These results compare qualitatively well with the results reported in References [26, 27] and the photographs included in [28]. In computations of this problem with the MLIT, the interface mesh undergoes severe distortions, and the computations cannot be continued without remeshing of the interface.

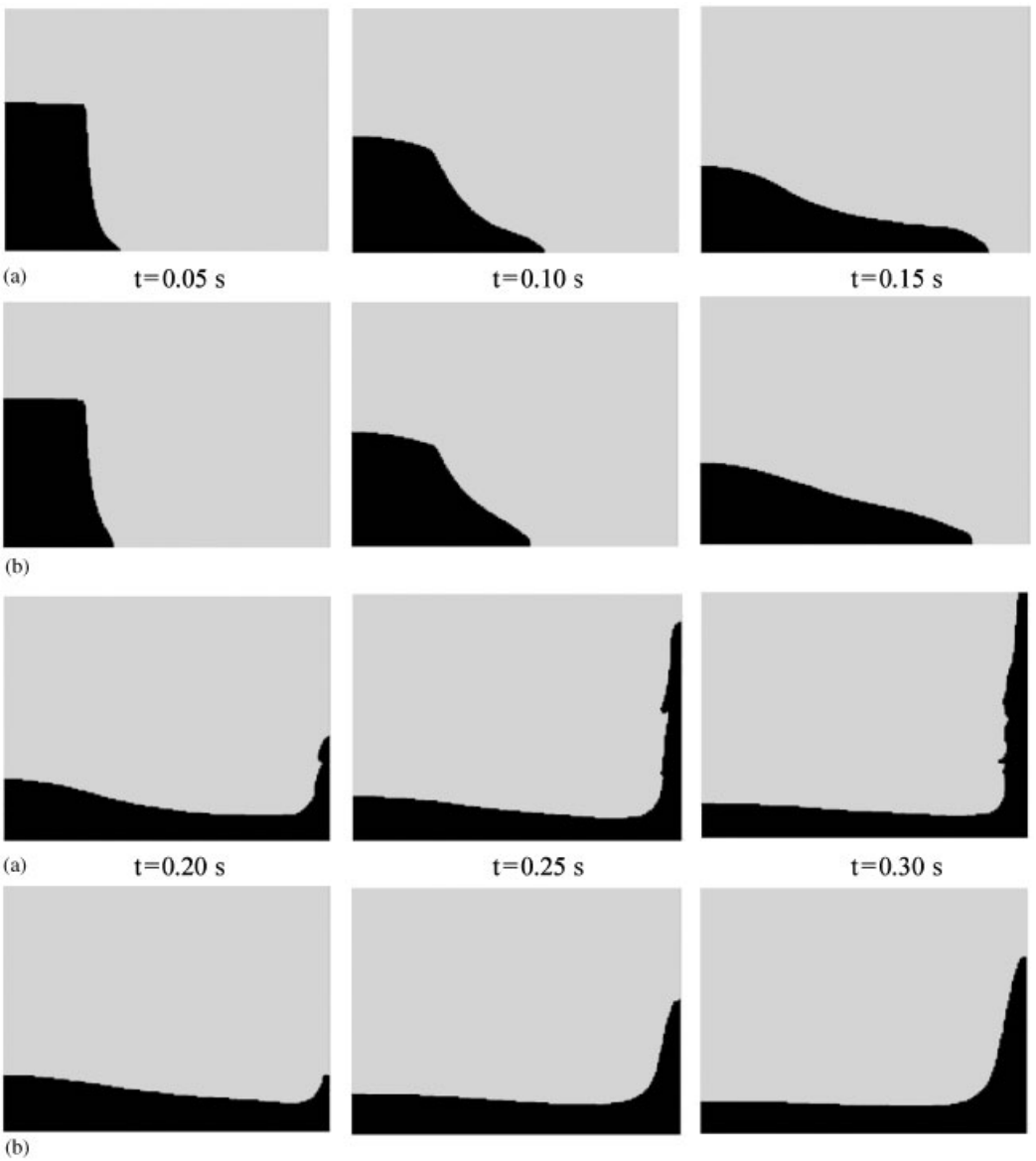

Figure 12. Collapse of a liquid column in a closed receptacle. Interface positions at various instants, obtained with: (a) the ETILT, and (b) the ETILT/TM.

3.4. Bore problem

The bore problem was presented in Reference [24] to evaluate numerical performance in dealing with highly unsteady problems. The layout of the idealized problem is shown in Figure 14. A horizontal layer of water with initial depth of h_0 is pushed back to the wall at one end with a

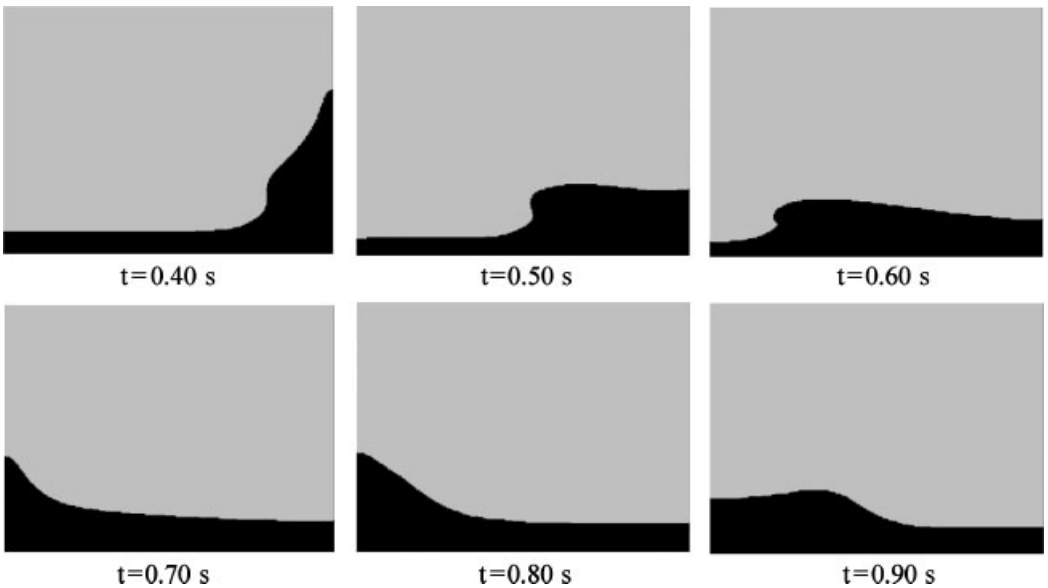

Figure 13. Collapse of a liquid column in a closed receptacle. Interface positions at various instants, obtained with the ETILT/TM.

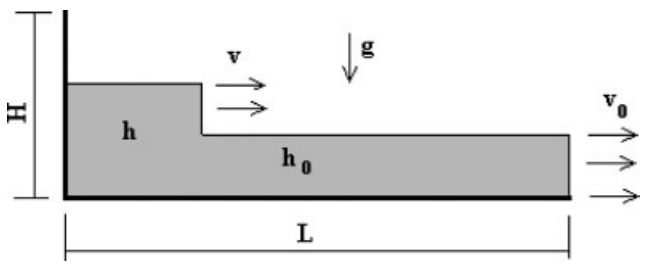

Figure 14. Bore problem. Layout of the idealized problem.

velocity of v_0 applied at the other end. This generates a hydraulic jump that runs away from the wall with a wave height of h and wave speed of v. We set $h_0 = 0.10\,\text{m}$ and $v_0 = -0.2971\,\text{m/s}$, and use a computational domain with dimensions $L = 0.75\,\text{m}$ and $H = 0.30\,\text{m}$. The fluid properties used in the computations are, $\rho_1 = 1000\,\text{kg/m}^3$, $\mu_1 = 0.001\,\text{kg/m/s}$, $\rho_2 = 1\,\text{kg/m}^3$, and $\mu_2 = 0.001\,\text{kg/m/s}$. Slip conditions are assumed at the solid boundaries, and the pressure is set to zero at the top of the computational domain. We use the same turbulence model that we had in Section 3.3, with the only difference being in the value of the mixing length, which is set here as $l_{\text{mix}} = 0.050\,\text{m}$. The finite element mesh is uniform and has 75×30 elements. The time step size is 0.001 s.

The interface positions at various instants, obtained with the ETILT/TM are shown in Figure 15. The water level at the left wall increases at the early stages. Once the bore is fully

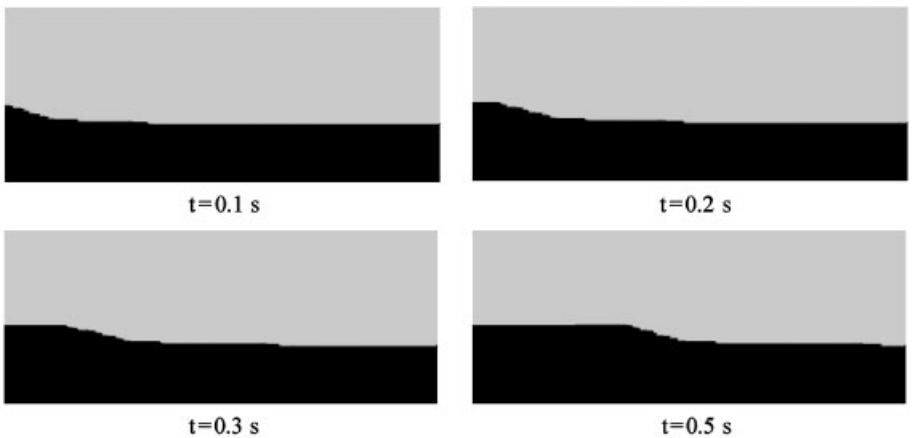

Figure 15. Bore problem. Interface positions at various instants, obtained with the ETILT/TM.

Table I. Bore problem. Mean values of the wave height and speed.

	Analytical	CSPH [24]	ETILT/TM
Wave height (m)	0.132	0.130	0.134
Wave speed (m/s)	0.928	0.910	0.900

developed, the wave height reaches a constant level. The interface profiles shown in Figure 15 are slightly different from those reported in Reference [24], mainly due to the different fluid properties used. Nevertheless, as it is shown in Table I, the predictions for the wave height and speed are in reasonably good agreement with those reported in Reference [24]. They are also in good agreement with the analytical values determined from the non-linear equations $v = v_0 + [gh(1 + h/h_0)/2]^{1/2}$ and $h/h_0 = (v - v_0)/v$.

4. CONCLUDING REMARKS

For computation of two-fluid interfaces, we presented an interface-capturing algorithm based on the ETILT. Because the technique is mostly node-based, managing the interface motion is easier than it is in an interface-tracking technique. Stabilized formulations are used in finite element discretizations of the both the Navier–Stokes equations and the advection equation governing the evolution of the interface function. The interface function marks the location of the interface. Based on also tracking the interface along the element edges, the technique is supplemented with mass-balance correction and interface-function reconstruction. With these enhancements, the technique possesses some of the desirable features of the interface-tracking techniques, namely the global mass conservation and the interface sharpness. With a number of test problems, we demonstrated the effectiveness of the technique. Our future research directions will include alternative projection algorithms for reconstructing the interface function;

mass conservation by directly correcting the interface locations along the element edges; and extending the technique, with its enhancements, to bubble and drop formations.

ACKNOWLEDGEMENTS

The supports provided by the Chilean Council for Research and Technology CONICYT (FONDECYT Projects Nos. 1020029 and 7020029) and the Department of Technological and Scientific Research at the Universidad de Santiago de Chile are gratefully acknowledged.

REFERENCES

1. Hughes TJR, Liu WK, Zimmermann TK. Lagrangian–Eulerian finite element formulation for incompressible viscous flows. *Computer Methods in Applied Mechanics and Engineering* 1981; **29**:239–349.
2. Huerta A, Liu W. Viscous flow with large free surface motion. *Computer Methods in Applied Mechanics and Engineering* 1988; **69**:277–324.
3. Tezduyar TE. Stabilized finite element formulations for incompressible flow computations. *Advances in Applied Mechanics* 1991; **28**:1–44.
4. Tezduyar TE, Behr M, Liu J. A new strategy for finite element computations involving moving boundaries and interfaces—the deforming-spatial-domain/space–time procedure: I. The concept and the preliminary tests. *Computer Methods in Applied Mechanics and Engineering* 1992; **94**(3):339–351.
5. Tezduyar TE, Behr M, Mittal S, Liu J. A new strategy for finite element computations involving moving boundaries and interfaces—the deforming-spatial-domain/space–time procedure: II. Computation of free-surfaces flows, two-liquid flows, and flows with drifting cylinders. *Computer Methods in Applied Mechanics and Engineering* 1992; **94**(3):353–371.
6. Thompson E. Use of pseudo-concentrations to follow creeping viscous flows during transient analysis. *International Journal for Numerical Methods in Engineering* 1986; **6**:749–761.
7. Sethian JA. Evolution, implementation, and application of level set and fast marching methods for advancing fronts. *Journal of Computational Physics* 2001; **169**:503–555.
8. Dhatt G, Gao DM, Ben Cheikh A. A finite element simulation of metal flow in moulds. *International Journal for Numerical Methods in Engineering* 1990; **30**:821–831.
9. Codina R, Soto O. A numerical model to track two-fluid interfaces based on a stabilized finite element method and the level set technique. *International Journal for Numerical Methods in Fluids* 2002; **40**:293–301.
10. Kim MS, Lee WI. A new VOF-based numerical scheme for the simulation of fluid flow with free surface. Part I: new free surface-tracking algorithm and its verification. *International Journal for Numerical Methods in Fluids* 2003; **42**:765–790.
11. Lewis RW, Ravindran K. Finite element simulation of metal casting. *International Journal for Numerical Methods in Engineering* 2000; **47**:29–59.
12. Tezduyar TE. Finite element methods for flow problems with moving boundaries and interfaces. *Archives of Computational Methods in Engineering* 2001; **8**:83–130.
13. Tezduyar TE. Interface-tracking and interface-capturing techniques for computation of two-fluid flows. *Proceedings of the First MIT Conference on Computational Fluid and Solid Mechanics*, Boston, MA, 2001.
14. Tezduyar T. Finite element interface-tracking and interface-capturing techniques for flows with moving boundaries and interfaces. *ASME Paper IMECE2001/HTD-24206. Proceedings of the ASME Symposium on Fluid-Physics and Heat Transfer for Macro- and Micro-Scale Gas-Liquid and Phase-Change Flows* (CD-ROM). ASME: New York, 2001.
15. Tezduyar TE. Stabilized finite element formulations and interface-tracking and interface-capturing techniques for incompressible flows. In *Numerical Simulations of Incompressible Flows*, Hafez MM (ed.). World Scientific: New Jersey, 2003; 221–239.
16. Cruchaga M, Oñate E, Idelsohn S. On the pseudomaterial approach for the analysis of transient forming processes. *Communications in Numerical Methods in Engineering* 1995; **11**:137–148.
17. Cruchaga MA, Oñate E. A finite element formulation for incompressible flow problems using a generalized streamline operator. *Computer Methods in Applied Mechanics and Engineering* 1997; **143**:49–67.
18. Cruchaga MA, Oñate E. A generalized streamline finite element approach for the analysis of incompressible flow problems including moving surfaces. *Computer Methods in Applied Mechanics and Engineering* 1999; **173**:241–255.
19. Cruchaga M, Celentano D, Tezduyar T. A moving Lagrangian interface technique for flow computations over fixed meshes. *Computer Methods in Applied Mechanics and Engineering* 2001; **191**:525–543.

20. Cruchaga M, Celentano D, Tezduyar T. Computation of mould filling processes with a moving Lagrangean interface technique. *Communications in Numerical Methods in Engineering* 2002; **18**:483–493.
21. Tezduyar TE. Finite elements methods for fluid dynamics with moving boundaries and interfaces. *Encyclopedia of Computational Mechanics*, 2004, to appear.
22. Tezduyar TE. Stabilized finite elements methods for flows with moving boundaries and interfaces. *HERMIS International Journal*, 2004, to appear.
23. Tezduyar TE. Moving boundaries and interfaces. *Finite Element Methods*: *1970's and Beyond*, 2004, to appear.
24. Bonet J, Look T. Variational and momentum preservation aspects of smooth particle hydrodynamic formulations. *Computer Methods in Applied Mechanics and Engineering* 1999; **180**:97–115.
25. Martin J, Moyce W. An experimental study of the collapse of liquid columns on a rigid horizontal plane. *Philosophical Transactions of the Royal Society of London* 1952; **244**:312–324.
26. García V, Muñoz-Cobo J, López L. Use of high accuracy schemes to handle free surfaces in computing unsteady two-phase flows. *Computer Methods in Applied Mechanics and Engineering* 1998; **162**:271–286.
27. Idelsohn S, Storti M, Oñate E. Lagrangian formulations to solve free surfaces incompressible inviscid fluid flows. *Computer Methods in Applied Mechanics and Engineering* 2001; **191**:583–593.
28. Koshizuka S, Tamako H, Oka Y. A particle method for incompressible viscous flow with fluid fragmentation. *Journal of Computational and Fluid Dynamics* 1995; **4**:29–46.

